MINIREVIEW

Check for updates

Opportunities and challenges in perovskite–organic thin-film tandem solar cells

Xin Meng, [a,b,c] Zhengrong Jia, [a,b] Xiuxiu Niu, [a,b] Chunnian He [ID] *[c,d] and Yi Hou [ID] *[a,b]

Efficiency is paramount in enhancing the performance and cost-effectiveness of solar cells. Recent advancements in single-junction perovskite solar cells (PSCs) have yielded an impressive efficiency of 26.1%, nearing their theoretical limit. Meanwhile, multi-junction tandem solar cells exhibit a remarkable efficiency potential exceeding 42%, surpassing the 33% limit of single-junction cells, thereby opening avenues for ultra-high-efficiency solar cells. Tandem solar cells (TSCs) represent a groundbreaking photovoltaic technology, offering high efficiency, low cost, and a simple fabrication process. Among various TSCs, perovskite–organic TSCs (PO TSCs) are particularly promising due to their ability to leverage the complementary strengths of PSCs and organic solar cells (OSCs). PO TSCs are poised to outperform existing TSCs in terms of device performance, manufacturing cost, and diverse applications. The introduction of Y6-series non-fullerene acceptors (NFAs) over the past three years has significantly advanced the development of OSCs, leading to remarkable progress in PO TSCs. This paper commences by elucidating the advantages and potential of OSCs as bottom sub-cells in PO TSCs, followed by an in-depth review of mainstream interconnection layer (ICL) design. It then addresses key challenges in wide bandgap PSCs, including phase segregation, photovoltage loss, energy loss, and long-term stability. The paper concludes by examining critical factors influencing the future development of PO TSCs.

Introduction

Since the initial introduction of perovskite materials as the absorbing layer in photovoltaic devices, achieving a power conversion efficiency (PCE) of 3.8%, metal–halide perovskite solar cells (PSCs) have witnessed a remarkable leap in efficiency in recent decades. The latest single-junction PSCs have reached a certified PCE of 26.1%, on par with silicon solar cells and are nearing their theoretical maximum efficiency, known as the Shockley–Queisser limit, of about 33%. This has brought tandem solar cells (TSCs) into the spotlight, offering the potential to surpass this limit with efficiencies over 40%.[1]

The operational framework of TSCs remains consistent across various designs: the top wide-bandgap sub-cell absorbs high-energy photons, while the bottom narrow-bandgap subcell captures low-energy photons. In two-terminal (2-T)

[a]Department of Chemical and Biomolecular Engineering, National University of Singapore, 117585, Singapore. E-mail: yi.hou@nus.edu.sg
[b]Solar Energy Research Institute of Singapore (SERIS), National University of Singapore, 117574, Singapore
[c]Joint School of National University of Singapore and Tianjin University, International Campus of Tianjin University, Fuzhou, China
[d]School of Materials Science and Engineering, Tianjin Key Laboratory of Composite and Functional Materials, Tianjin University, Tianjin 300350, China. E-mail: cnhe08@tju.edu.cn

systems, the integration of an optically transparent interconnecting layer (ICL) is indispensable for electrically amalgamating these two sub-cells, with ICLs playing a vital role in optimizing the overall TSC performance.[2] Perovskite-based thin-film TSCs have undergone significant improvements attributed to the tunable bandgap of PSCs through composition engineering. All-perovskite TSCs have achieved a PCE of 29.4%,[3] surpassing the previously reported efficiencies of single-junction silicon (Si) and PSCs. Nevertheless, Sn–Pb-based PSCs suffer from oxidative instability of the Sn^{2+} cation, adversely affecting long-term stability in all-perovskite TSCs.

Organic solar cells (OSCs), with their vast chemical design space, strong absorption coefficient around the near-infrared (NIR) range, non-toxicity, flexibility, and solution processability, are emerging as promising narrow-bandgap sub-cells in tandem with wide-bandgap PSCs. The first introduction of perovskite–organic tandem solar cells (PO TSCs) did not stir up much excitation due to their huge backwardness of efficiency compared with other tandem counterparts.[4] However, the emergence of Y6-series non-fullerene acceptors (NFAs) ignited the progress of OSCs. The first reported PO TSCs employing a PM6–Y6 binary blend as the organic sub-cell achieved a PCE exceeding 18%.[5] Additionally, similar tandem structure devices with all-inorganic perovskite sub-cells presented over 18% efficiency.[6] Subsequent surface passivation of the perovskite sub-cells with trimethylammonium chloride pushed PO

TSCs to a PCE of 21.4%.[7] Recently, the incorporation of a fullerene derivative, [6,6]-phenyl-C_{61}-butyric acid methyl ester ($PC_{61}BM$), into the PM6–Y6 binary blend to form a ternary system yielded PO TSCs with a remarkable PCE of 24%.[8] Over the past three years, the efficiency of PO TSCs has surged from 15.9%[9] to nearly 24%,[8] underscoring their competitive potential in tandem applications. This surge in interest and performance, particularly since the advent of Y6-series based OSCs in 2019, coupled with advancements in wide-bandgap PSCs, has significantly propelled the development of PO TSCs. Further enhancement in the performance of POTSC necessitates deeper research into the narrow-bandgap organic layer and interconnecting layer to the wide-bandgap perovskite layer.

Organic solar cells: a promising tandem bottom cell

Over the years, research has aimed to boost the efficiency of OSCs. Their near-limitless chemical space for designing molecular donors and acceptors presents significant potential. Innovations in materials and device configurations have propelled efficiencies of OSCs from 3% to 19%,[3] as depicted in Fig. 1a.

Yi Hou holds the position of Presidential Young Professor within the Department of Chemical and Biomolecular Engineering at the National University of Singapore (NUS). In September 2020, he was appointed as the Head of the Perovskite-based Multijunction Solar Cell Group at the Solar Energy Research Institute of Singapore (SERIS). His academic journey includes the completion of a Ph.D. in Materials Science

Yi Hou

and Engineering from the University of Erlangen-Nuremberg in Germany. Following that, he pursued postdoctoral training at the University of Toronto's Department of Electrical and Computer Engineering. Yi was recognized as one of the Innovators Under 35 (Asia Pacific) by MIT Tech Review due to his contributions to advancing perovskite-based tandem solar cell technology. In 2022, his achievement in setting a world record for the efficiency of a perovskite/organic tandem solar cell was documented in the "Solar cell efficiency tables (Version 60)." In 2023, the Hou group set a new world record for single-junction perovskite solar cell efficiency (1 cm²), recognized in "Solar cell efficiency tables (Version 62)." Yi has been named a Clarivate Analytics Highly Cited Researcher in the Cross-Field category for the second consecutive year, from 2022 to 2023.

In the last decade, research on OPVs has increasingly concentrated on developing new donor materials and NFAs. Notably, A–D–A-type NFAs, especially ITIC based on small-molecular fused rings, improved the efficiency from 4% to 14%.[10–14] These NFAs, capable of absorbing red and infrared light, have revolutionized OSCs. A blend of Y6 and PM6, for instance, achieved over 15% efficiency in early 2019.[15] The introduction of the A–DA'D–A-type Y6-series further propelled device efficiency beyond 19% in less than three years.[16–22] A summary of the photovoltaic performance of OSCs using NFAs from recent works is shown in Table 1.

A distinctive advantage of OSCs is their ability to tune and selectively absorb light in the NIR spectrum, essential for achieving higher short-circuit current density (J_{SC}) by capturing low-energy infrared photons. NIR photovoltaic materials, including p-type polymers and n-type fullerenes and non-fullerenes, can be categorized into specific absorption ranges, with D–A units and intramolecular charge transfer (ICT) playing a key role. The design of these units, based on their electron-donating and -withdrawing abilities, influences the absorption window (Fig. 1b).[23]

The broad design flexibility in OSCs promises tunable absorption spectra and energy levels, making them ideal for tandem solar cell applications. Their strong absorption coefficient in the NIR range, compared to Si perovskite and CIGS inorganic solar cells, positions them as excellent candidates for bottom sub-cells in tandem solar cells. Thus, the thickness of the bottom cells in PO TSCs is significantly reduced compared to silicon-perovskite and perovskite–perovskite TSCs, indicating the potential for flexible, large-scale modules[28–31] (Fig. 1c and d). The optimized active layer films, with partial light transparency and tunable color, are suitable for semiconductor solar cells and have applications in wearable energy resources and building-integrated photovoltaics.

However, the stability of OSCs, particularly when exposed to ultraviolet (UV) light, remains a concern. While single OSCs exhibit instability, the UV filtering effect (Fig. 1e) of wide-bandgap perovskite sub-cells in PO TSCs improves the overall long-term stability of these devices compared with the single OSCs, as shown in Fig. 1f.[8,24–27] This contrast is particularly notable in comparison with all-perovskite TSCs, which struggle with the instability of Sn-based perovskite sub-cells. The improved stability of PO TSCs, demonstrated under various illumination conditions, suggests a promising future for these devices, combining efficient energy harvesting with long-term operational stability.

Design of the interconnection layer for tandem solar cells

Achieving ideal current matching in monolithic TSCs is crucial, where each sub-cell should absorb and convert the same number of photons into electrons without significant photovoltage loss. This necessitates precise band alignment. Typically, photogenerated electrons move to a lower conduc-
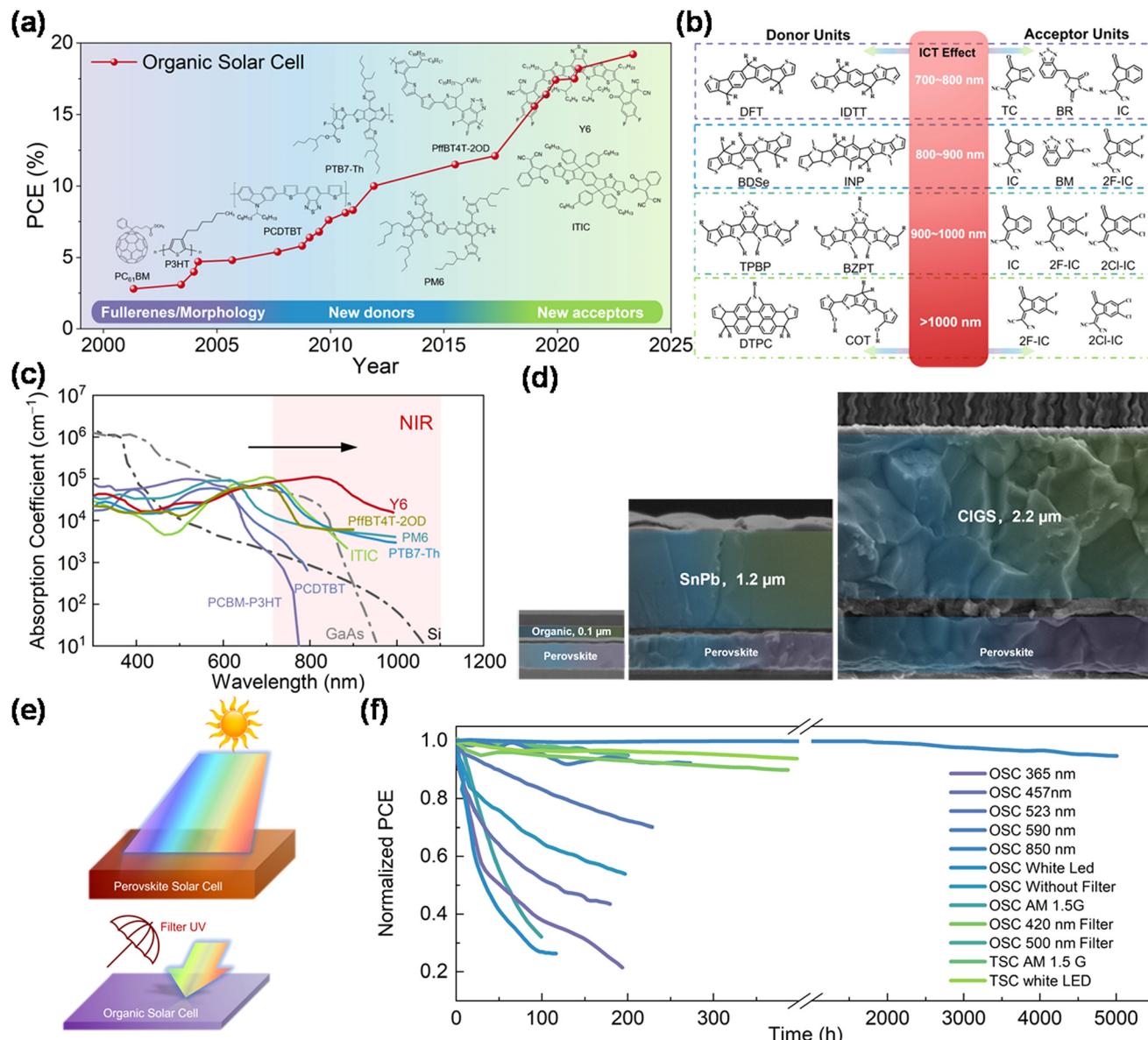
Fig. 1 (a) Highest certified efficiency evolution of OSCs from the National Renewable Energy Laboratory (NREL) (USA).[3] (b) Electron-donating donor units and electron-withdrawing acceptor units with ICT effects to redshift the absorption window. Reproduced from ref. 23 with permission from Wiley-VCH GmbH, copyright 2022. (c) Adsorption coefficient of different solar cells (Si, GaAs, and a series of organic solar cells) within the NIR region. (d) Thickness of perovskite–organic, all-perovskite, and perovskite–CIGS TSCs as compared by SEM. Reproduced from ref. 27 with permission from Springer, copyright 2022. Reproduced from ref. 32 with permission from Springer, copyright 2022. Reproduced from ref. 33 with permission from American Chemical Society, copyright 2022. (e) Schematic diagram of the UV filtering effect of wide-bandgap PSCs to protect OSCs. (f) Operational stability of PM6 and Y6-based OSCs comprising illumination either with broadband spectra (white LED or AM1.5) or with monochromatic light sources.

tion band, and holes migrate to a higher valence band, as illustrated in Fig. 2a. In TSCs, n-type layers often have a lower work function, while p-type layers have a higher one, creating a barrier that can limit current flow. To address this, two main strategies are employed: one involves introducing a recombination layer with high electrical conductivity to provide more sites for electron–hole recombination[41,42] and the other uses heavily doped n-type (n+++) and p-type (p+++) layers to form a tunnel junction for enhanced recombination (Fig. 2a).[43] These

strategies help transfer charge carriers between sub-cells and recombine them, although interface recombination can create opposite-sign voltage, reducing the open-circuit voltage (V_{OC}) of tandem devices.

The ICL is critical for the overall performance of TSCs. An ideal ICL provides ohmic contact for efficient charge extraction and sufficient recombination sites to minimize potential loss.[44] Typically, the ICL connects the electron extraction layer of a wide-bandgap perovskite layer with the hole extraction

Table 1 Summary of the photovoltaic performance of OSCs using NFAs from recent works

NFA	E_g (eV)	HOMO/LUMO (eV)	V_{OC} (V)	J_{SC} (mA cm^{-2})	FF (%)	PCE (%)	Ref.
PM6-Tz40:Y6	—	−5.61/−3.58	0.85	25.3	0.72	15.5	34
PM6–Y6	1.33	−5.56/−3.50	0.83	25.3	74.8	15.7	15
PBTT-F:Y6	1.33	−5.65/−3.68	0.84	24.8	77.1	16.1	35
S1:Y6	1.41	−5.65/−3.72	0.877	25.402	0.737	16.421	36
PTzBI-dF:Y6	1.34	−5.68/−3.58	0.85	26.33	75.5	16.8	37
PM7:Y6	1.42	−5.60/−3.57	0.882	25.605	73.3	17.037	38
PM6-Tz20:Y6	—	−5.61/−3.59	0.86	27.3	0.75	17.6	34
D18:Y6Se	—	−5.72/−4.15	0.839	27.98	0.753	17.7	39
D18-Cl:Y6:G19	1.3	−5.71/−3.45	0.871	27.36	77.72	18.53	40
PM1:L8-BO:BTO-2F2Cl	1.428	−5.76/−3.60	0.881	27.15	80.14	19.17	17
PM6:D18:L8-BO	—	−5.67/−2.95	0.896	26.7	81.9	19.6	19
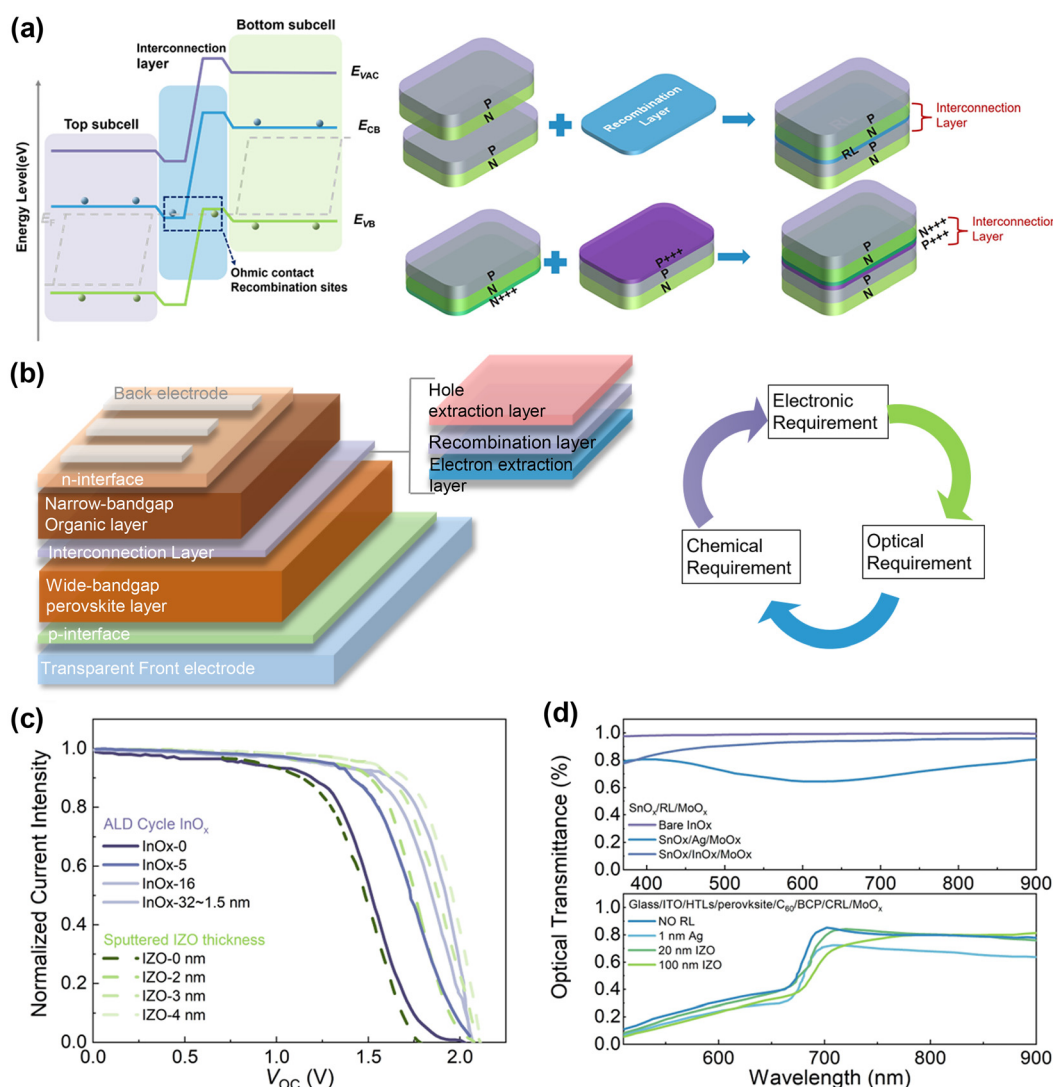
Fig. 2 (a) Energy level diagram of TSCs and schematic diagram of two individual sub-cells connected by an ICL with a recombination layer configuration and connected by an ICL with a tunnel junction configuration. (b) Typical device structure of 2-T PO TSCs and donut chart of the ICL in terms of electronic, optical, and chemical requirements. (c) J−V characteristic curves of PO TSCs with different thicknesses of metal oxide interconnects. Reproduced from ref. 8 with permission from Springer, copyright 2022. Reproduced from ref. 27 with permission from Springer, copyright 2022. (d) Optical transmittance of the metal oxide RL within a sandwich charge extraction layer structure and PO tandem structure. Reproduced from ref. 8 with permission from Springer, copyright 2022. Reproduced from ref. 27 with permission from Springer, copyright 2022.

layer of a narrow-bandgap organic layer (Fig. 2b).[45,46] Besides electrical requirements, a qualified ICL should be optically transparent, particularly in the NIR range, to avoid parasitic absorption that can decrease the J_{SC} of the bottom sub-cells. From a chemical perspective, the ICL should protect the bottom sub-cells during solvent-involved deposition steps. Fortunately, the use of orthogonal solvents for the organic and perovskite sub-cells relaxes some of these chemical protection requirements. However, deposition conditions need to be gentle to avoid damaging underlying cells.[44,47]

High-efficiency PO TSCs typically use ICLs comprising an n-type electron extraction layer like SnO_x, a hole extraction layer like MoO_x and an ultra-thin carrier recombination layer (RL).[8] However, the significant work function difference between SnO_x and MoO_x can create a Schottky barrier, hindering recombination and leading to poor photovoltaic performance. One solution is to insert a thin metal layer like Ag to facilitate recombination (first-generation ICL), but this can reduce ICL transmittance and limit light absorption in the organic sub-cells.[27] Another alternative is using metal oxides like indium oxide or doped indium zinc oxide (IZO), which offer better optical and electrical properties and can lead to record PCEs in PO TSCs.

The thickness of the ICL in TSCs is closely linked to its carrier modulation capability, a key factor for the practical functionality of these cells. Varying the thickness of the ICL directly influences its ability to modulate carriers, as demonstrated by differing J–V characteristic curves observed for various thicknesses of indium oxide (InO_x) and IZO recombination layers (Fig. 2c).[8,27] Generally, a thinner ICL is advantageous due to larger sheet resistance, which helps avoid potential shunting paths between sub-cells and within the TSC structure itself. The ultra-thin InO_x layer, deposited using atomic layer deposition (ALD), proves more beneficial than thicker, more conductive IZO layers in this regard. In addition, we presented the electrical conductivity of the present commonly utilized ICL materials as shown in Table 2.[48,49] Optically, a thinner ICL reduces parasitic absorption, thereby diminishing optical losses that could severely affect the external quantum efficiency of the cells (Fig. 2d).[8] InO_x layers, for example, maintain transparency across a wide range of optical absorptions, unlike ultra-thin metal layers such as silver, which show significant optical loss. This transparency is crucial for minimizing the impact on the external quantum efficiency of the device.

Moreover, PO TSCs with a thin IZO layer demonstrate excellent transmittance in the 700 to 950 nm wavelength range,

optimizing the NIR photon absorption for Y6-series NFAs. Utilizing metal oxides as RLs thus enhances the external quantum efficiency of rear sub-cells in the TSCs.[27]

While the second-generation metal–oxide RLs show promise for high-performance PO TSCs, challenges remain in their deposition. Techniques like sputtering, thermal evaporation, and ALD face barriers in creating homogeneous, large-area layers with sub-nanometer thickness. Moreover, the high energy used in these processes may damage the underlying sub-cells. Exploring suitable fabrication methods for these metal oxide ICLs is crucial for advancing high-performance PO TSCs, including large-scale modules.

Phase segregation and photovoltage plateau of wide-bandgap PSCs

The ability to engineer the composition of perovskite materials allows for tuning their bandgap from 1.2 eV to 2.5 eV, effectively covering the entire visible solar spectrum. Typically, altering the bandgap involves substituting halide ions, such as Br and Cl.[50] Cs/MA- and Cs/FA-based perovskite materials, known for their stability, are preferred in modern perovskite-based TSCs over pure MA- or FA-based materials. Enlarging the bandgap of perovskites by increasing the Br ion concentration is common, with bandgaps over 1.85 eV being ideal for perovskite sub-cells in PO TSCs. This is due to their compatibility with the bandgaps of advanced NFAs from OSCs, which typically range between 1.25 and 1.35 eV.[51]

However, mixed halide perovskites with a high Br content often exhibit phase segregation. This results in the division of the perovskite phase into iodine-rich and bromine-rich domains under light exposure, as depicted in Fig. 3a. A significant issue with mixed halide perovskites, particularly those with high halide concentration, is V_{OC} loss. Theoretically, V_{OC} should increase with a larger bandgap, but a photovoltage plateau occurs when the Br concentration surpasses 20%, as shown in Fig. 3b.[47]

Various models, including thermodynamics, lattice strain, charge-trapping-induced electric fields, and discrepancies between different perovskite phases, have been explored to understand phase segregation and its mechanisms. Density functional theory (DFT) calculations indicate that the formation energy of bromine vacancies (V_{Br^+}) is lower than that of iodine vacancies (V_{I^+}).[50] According to charge dynamics theory, hybrid perovskites exhibit a high static dielectric constant, leading to strong electron–phonon coupling, increased polarizability, and reduced exciton binding. This results in the quick dissociation of photogenerated electron–hole pairs into free carriers, causing distortion in the perovskite lattice, which affects its enthalpy and free energy. Phase segregation is driven by the migration of halide ions, facilitated by halide defects at surfaces or grain boundaries. For instance, ion migration in $MAPbI_3$ occurs more rapidly at grain boundaries than within grains.[52]

Table 2 Summary of the electrical conductivity of common ICL materials

ICL materials	Electrical conductivity (S cm^{-2})	Ref.
Ag	0.568	48
Au	0.426	48
SnO_x	0.122	48
MoO_x/Ag	2.306	49
ZnO/Ag/MoO_x	1.593	49
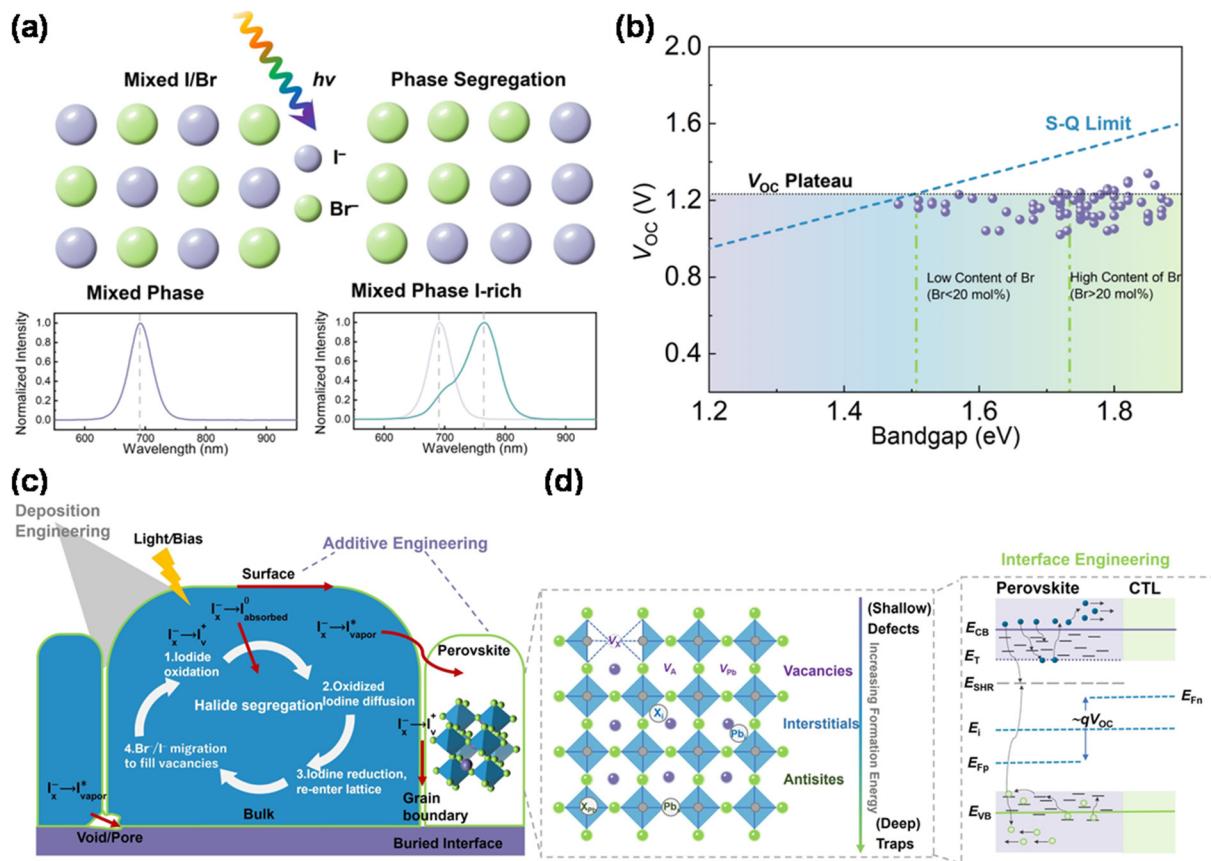
Fig. 3 (a) Schematic diagram of the process of light–induced halide segregation corresponding to the measured photoluminescence results of the pristine phase and segregated phase. (b) Evolution summary graph of V_{OC} for contemporary wide-bandgap PSCs and the commonly observed photovoltage plateau. Reproduced from ref. 47 with permission from Elsevier, copyright 2023. (c) Possible mechanism diagram of phase segregation related to iodide oxidation/reduction and transport pathways. (d) Schematic diagram of deposition, composition, additive, and interface engineering from the energy level and trap state.

Recently, the study of halide oxidation has marked a significant breakthrough in understanding phase segregation within wide-bandgap perovskites. Rand *et al.* noticed that halide oxidation takes a leadership role in the physical demixing of mixed halide compositions, and it is a critical step to initiate the halide segregation, followed by underlying thermodynamic and kinetic driving forces to worsen this situation.[53] This model involves four major steps; first, iodide on the perovskite surface is oxidized allowing it to leave the lattice as oxidized iodine products, which will introduce a halide vacancy (V_X) as shown in Fig. 3c. Second, these oxidized species simultaneously diffuse across through perovskite bulks, surfaces, or pores/voids. Then, these oxidized iodine products will reduce at vacant surface sites to re-enter the halide lattice. Finally, halide anions will diffuse under light excitation or drift under bias driving to neutralize this V_X sourced from the surface iodide loss. The spatial variation of iodide oxidation and reduction forces will eventually yield iodide-rich domains. Notably, triggers from light, electrical bias, and thermal stresses are synergistic and complex effects, and more evidence and advanced *in situ* characterization tools are needed to verify the suitability of this model.[54]

Phase segregation is regularly recognized to contribute to the V_{OC} deficit, due to carriers funneling from Br rich to I rich domains to limit the quasi-Fermi level splitting.[55,56] Yet, given that V_{OC} is extracted from the *J–V* curves usually measured within around 10 s, the phase segregation may not activate to affect the V_{OC} during this transient moment.[57] Recently, V_{OC} loss has been attributed to the trap-assisted non-radiative recombination of the free carriers through the perovskite bulk, surface, and interface.[55] The work function and quality of the perovskite layer/transport layer interface of the charge transport layer impact the V_{OC} of devices.[57] Thus, the energy level alignment between the perovskite layer and carrier transport layer (CTL) is key to the issue. The inappropriate interface energy, mismatched interface energy level, and poor carrier transport layer will induce serious V_{OC} loss. The poor film quality indicates that there exists a lot of defects in the perovskite, especially at the surface and grain boundaries, to trap carriers. These trapped charges may escape and be collected by the electrode for a long time, so may not significantly affect the photocurrent output, whereas the resulting energy disorder and low carrier concentration will significantly reduce the V_{OC}. Herein, it is essential to utilize composition engineering and deposition engineering to obtain high-quality perovskite films to avoid intrinsic defects within the perovskite, as shown in Fig. 3c.[58–61]

These defects can be classified from shallow defects (ionic vacancies) to deep traps (interstitials and anti-site substitutions) with increasing defect formation energy, where an increase in its formation energy corresponds to a decrease in the probability of occurrence.[62–64] These defects can act as charge recombination centers (trap states) to trap the charge carrier to decrease the photovoltage of devices.[65] Shallow traps, such as iodide vacancies, involved in phase segregation can be undermined through additive engineering to neutralize these defects around the grain boundaries of PSCs. Metal halide ions, such as Rb^+,[66] Cs^+[67] and Sn^{2+},[68] can be added into the perovskite precursor to incorporate with defeats within the perovskite, as well passivate grain boundaries with K^+ addition.[69] Furthermore, adding SCN^-[70–72] into the perovskite precursor is a common method to increase the grain size and crystallinity of the perovskite. In addition, the positions of these traps are dependent on the energy level of the conduction band minimum (CBM) and valence band maximum (VBM). Combined with the types of these defects and further focus on the energy levels of the perovskite/CTL interface (Fig. 3d), it is obvious that the wide distribution of traps and energy disorder between the perovskite/CTL interface can reduce the quasi-Fermi levels of photogenerated electrons and holes (E_{Fn}, E_{Fp}), thereby reducing the device V_{OC}.[73,74,78] Therefore, considering the trapped defects of the perovskite/charge transport layer interface, effective passivation of the interface is essential to reduce the charge defect density and extend the carrier recombination lifetime to achieve low V_{OC} loss. Many efforts have been made to explore interface engineering from self-assembled monolayers and passivation of the perovskite surface and grain boundaries, to inserting low-dimensional layers to construct interfacial heterostructures, aiming to eliminate this non-radiative recombination from defects and traps and energy disorder from energy level mismatching.[75–77] For instance, benzylamine,[77] phenylethylamine bromide,[78] and guanidinium bromide[79] have been employed to construct interfacial 2D/3D heterostructures to passivate defects and inhibit ion migration.

The principles to achieve low V_{OC} loss include: (i) preparing high-quality perovskite layers with low defect density; (ii) inserting appropriate interface layers to achieve defect passivation on the surface; (iii) screening out perovskite layers with a virtuous energy level matching charge transport layer to evade the energy disorder issue at the interface.

Outlook and prospects

In the last five years, the PCEs of PO TSCs have soared from under 15%[9] to 24%,[8] showcasing remarkable potential in the field of photovoltaics. This impressive progress is attributable to advancements in wide-bandgap PSCs, ICLs, and narrow-bandgap OSCs. With ongoing research efforts to enhance metal halide perovskite and donor/acceptor organic materials, there is a strong belief that PO TSCs will continue to improve. The expectation is that PO TSCs will surpass the S–Q limit and

align with the performance of other leading perovskite-based TSCs, through step-by-step optimization of the sub-cells, ICLs, and optical management (Fig. 4).

For eventual commercialization, bridging the efficiency gap between lab-level devices and large-scale modules and boosting long-term operational stability are crucial, especially from an upscaling perspective. PO TSCs have shown potential in being applied to ultra-thin and large-scale modules. Future research should therefore focus not only on enhancing the efficiency and longevity of perovskite and organic sub-cells, developing innovative ICL structures and materials but also on exploring scalable fabrication methods for PO TSCs.

Despite advancements, the performance development of PO TSCs has lagged behind all-perovskite, perovskite–silicon, and perovskite–CIGS counterparts. Notably, while PO TSCs achieve comparable V_{OC} and FF to perovskite–silicon and all-perovskite TSCs, their J_{SC} is considerably lower. This is attributed to the larger bandgap of advanced Y6-series NFAs compared to Si and Sn–Pb-based sub-cells. Y6 materials, despite their limitations in EQE and energy loss, have yet to be surpassed by newer NFAs in OSCs. To address this, designing novel NFAs with a photo-response beyond 1000 nm in the NIR spectrum, efficient charge transport, and minimized energy loss is essential. Additionally, improving the luminescence efficiency at the interface charge transporting state through hybridization with emissive localized singlet excitons can enhance radiative recombination. Fine-tuning the molecular geometry, excited state symmetry, and orientation at the donor/acceptor interface are viable strategies for this purpose. Exploiting triplet properties from organic light-emitting diode technology could also offer insights.

The observed halide segregation and photovoltage loss in wide-bandgap perovskite films, which lead to energy losses
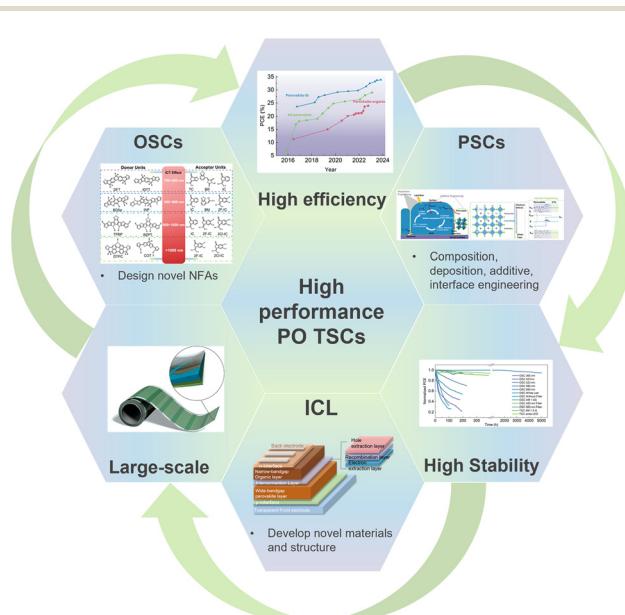
Fig. 4 Schematic diagram of the outlook and prospects for high-performance PO TSCs.

through carrier funneling, necessitate using compositions, additives, and deposition engineering to control perovskite crystallization, promoting uniform nucleation and growth. Besides halide segregation, nonradiative recombination due to high-density surface and bulk defects, causing energy level mismatch, is another significant source of energy loss. A deeper understanding of deep trap states in mixed halide perovskites and reasons behind the energy level mismatch between the perovskite active layer and charge transport layer is vital for designing effective defect passivation strategies to reduce V_{OC} loss further. Developing non-destructive microscopy imaging techniques with atomic-scale resolution to characterize *in situ* halide layering and remixing behavior under various stimuli is crucial for a better understanding of phase segregation mechanisms.

Addressing phase segregation is crucial for the long-term stability of PO TSCs. This involves minimizing grain boundaries and passivating trap states around them to reduce ion and defect diffusion, thereby inhibiting phase segregation through various engineering methods. Additionally, the instability and morphological changes of organic molecules in OSCs under light and heat are key factors in PO TSC degradation. Therefore, selecting stable donor/acceptor materials and optimizing their ratios is essential.

The ICL significantly impacts the efficiency, operational stability, and scalability of PO TSCs. Ultra-thin metal layers, such as Ag and Au, and conductive metal oxide layers, such as InO_x and IZO, are current mainstream materials in TSCs. Moreover, developing RLs with well-aligned energy levels and inherently low energy disorder is crucial to minimize charge extraction barriers and maximize quasi-Fermi-level splitting. However, the optical transmittance effects of metal layers can disrupt the balance between electrical and optical properties. Thus, transparent conductive oxide layers with high transmittance and electrical properties are more promising candidates for RLs in PO TSCs.

Conflicts of interest

There are no conflicts to declare.

Acknowledgements

References

1 F. Meillaud, A. Shah, C. Droz, E. Vallat-Sauvain and C. Miazza, *Sol. Energy Mater. Sol. Cells*, 2006, **90**, 2952–2959.

2 F. Martinho, *Energy Environ. Sci.*, 2021, **14**, 3840–3871.

3 NREL, Best Research-Cell Efficiencies, **https://www.nrel.gov/pv/cell-efficiency.html**.

4 J. Liu, S. Lu, L. Zhu, X. Li and W. C. Choy, *Nanoscale*, 2016, **8**, 3638–3646.

5 S. Xie, R. Xia, Z. Chen, J. Tian, L. Yan, M. Ren, Z. Li, G. Zhang, Q. Xue, H.-L. Yip and Y. Cao, *Nano Energy*, 2020, **78**, 105238.

6 X. Wu, Y. Liu, F. Qi, F. Lin, H. Fu, K. Jiang, S. Wu, L. Bi, D. Wang, F. Xu, A. K. Y. Jen and Z. Zhu, *J. Mater. Chem. A*, 2021, **9**, 19778–19787.

7 W. Chen, D. Li, X. Chen, H. Chen, S. Liu, H. Yang, X. Li, Y. Shen, X. Ou, Y. Yang, L. Jiang, Y. Li and Y. Li, *Adv. Funct. Mater.*, 2021, **32**, 2109321.

8 K. O. Brinkmann, T. Becker, F. Zimmermann, C. Kreusel, T. Gahlmann, M. Theisen, T. Haeger, S. Olthof, C. Tuckmantel, M. Gunster, T. Maschwitz, F. Gobelsmann, C. Koch, D. Hertel, P. Caprioglio, F. Pena-Camargo, L. Perdigon-Toro, A. Al-Ashouri, L. Merten, A. Hinderhofer, L. Gomell, S. Zhang, F. Schreiber, S. Albrecht, K. Meerholz, D. Neher, M. Stolterfoht and T. Riedl, *Nature*, 2022, **604**, 280–286.

9 Y. Liu, L. A. Renna, M. Bag, Z. A. Page, P. Kim, J. Choi, T. Emrick, D. Venkataraman and T. P. Russell, *ACS Appl. Mater. Interfaces*, 2016, **8**, 7070–7076.

10 C. B. Nielsen, S. Holliday, H. Y. Chen, S. J. Cryer and I. McCulloch, *Acc. Chem. Res.*, 2015, **48**, 2803–2812.

11 G. Wang, F. S. Melkonyan, A. Facchetti and T. J. Marks, *Angew. Chem., Int. Ed.*, 2019, **58**, 4129–4142.

12 C. Lee, S. Lee, G. U. Kim, W. Lee and B. J. Kim, *Chem. Rev.*, 2019, **119**, 8028–8086.

13 Z. Genene, W. Mammo, E. Wang and M. R. Andersson, *Adv. Mater.*, 2019, **31**, e1807275.

14 A. Wadsworth, M. Moser, A. Marks, M. S. Little, N. Gasparini, C. J. Brabec, D. Baran and I. McCulloch, *Chem. Soc. Rev.*, 2019, **48**, 1596–1625.

15 J. Yuan, Y. Zhang, L. Zhou, G. Zhang, H.-L. Yip, T.-K. Lau, X. Lu, C. Zhu, H. Peng, P. A. Johnson, M. Leclerc, Y. Cao, J. Ulanski, Y. Li and Y. Zou, *Joule*, 2019, **3**, 1140–1151.

16 Q. Yue, W. Liu and X. Zhu, *J. Am. Chem. Soc.*, 2020, **142**, 11613–11628.

17 R. Sun, Y. Wu, X. Yang, Y. Gao, Z. Chen, K. Li, J. Qiao, T. Wang, J. Guo, C. Liu, X. Hao, H. Zhu and J. Min, *Adv. Mater.*, 2022, **34**, e2110147.

18 C. He, Y. Pan, Y. Ouyang, Q. Shen, Y. Gao, K. Yan, J. Fang, Y. Chen, C.-Q. Ma, J. Min, C. Zhang, L. Zuo and H. Chen, *Energy Environ. Sci.*, 2022, **15**, 2537–2544.

19 L. Zhu, M. Zhang, J. Xu, C. Li, J. Yan, G. Zhou, W. Zhong, T. Hao, J. Song, X. Xue, Z. Zhou, R. Zeng, H. Zhu, C. C. Chen, R. C. I. MacKenzie, Y. Zou, J. Nelson, Y. Zhang, Y. Sun and F. Liu, *Nat. Mater.*, 2022, **21**, 656–663.

20 Q. Liu, Y. Jiang, K. Jin, J. Qin, J. Xu, W. Li, J. Xiong, J. Liu, Z. Xiao, K. Sun, S. Yang, X. Zhang and L. Ding, *Sci. Bull.*, 2020, **65**, 272–275.

21 S. Li, C.-Z. Li, M. Shi and H. Chen, *ACS Energy Lett.*, 2020, **5**, 1554–1567.

22 Q. Wei, W. Liu, M. Leclerc, J. Yuan, H. Chen and Y. Zou, *Sci. China: Chem.*, 2020, **63**, 1352–1366.

23 D. Meng, R. Zheng, Y. Zhao, E. Zhang, L. Dou and Y. Yang, *Adv. Mater.*, 2022, **34**, e2107330.

24 S. Qin, C. Lu, Z. Jia, Y. Wang, S. Li, W. Lai, P. Shi, R. Wang, C. Zhu and J. J. A. M. Du, *Adv. Mater.*, 2022, **34**, 2108829.

25 P. Weitz, V. M. Le Corre, X. Du, K. Forberich, C. Deibel, C. J. Brabec and T. Heumüller, *Adv. Energy Mater.*, 2022, **13**, 2202564.

26 T. Liu, Q. C. Burlingame, M. R. Ivancevic, X. Liu, J. Hu, B. P. Rand and Y. L. Loo, *Adv. Energy Mater.*, 2023, **13**, 2300046.

27 W. Chen, Y. Zhu, J. Xiu, G. Chen, H. Liang, S. Liu, H. Xue, E. Birgersson, J. W. Ho, X. Qin, J. Lin, R. Ma, T. Liu, Y. He, A. M.-C. Ng, X. Guo, Z. He, H. Yan, A. B. Djurišić and Y. Hou, *Nat. Energy*, 2022, **7**, 229–237.

28 M. Topič, *Contemp. Mater.*, 2011, **2**, 94–102.

29 X. Liu, J. Wang, J. Peng and Z. Liang, *Macromolecules*, 2017, **50**, 6954–6960.

30 X. Ma, Y. Mi, F. Zhang, Q. An, M. Zhang, Z. Hu, X. Liu, J. Zhang and W. Tang, *Adv. Energy Mater.*, 2018, **8**, 1702854.

31 J. Wu, J. Lee, Y.-C. Chin, H. Yao, H. Cha, J. Luke, J. Hou, J.-S. Kim and J. R. Durrant, *Energy Environ. Sci.*, 2020, **13**, 2422–2430.

32 R. Lin, J. Xu, M. Wei, Y. Wang, Z. Qin, Z. Liu, J. Wu, K. Xiao, B. Chen, S. M. Park, G. Chen, H. R. Atapattu, K. R. Graham, J. Xu, J. Zhu, L. Li, C. Zhang, E. H. Sargent and H. Tan, *Nature*, 2022, **603**, 73–78.

33 M. Jošt, E. Köhnen, A. Al-Ashouri, T. Bertram, Š. Tomšič, A. Magomedov, E. Kasparavicius, T. Kodalle, B. Lipovšek, V. Getautis, R. Schlatmann, C. A. Kaufmann, S. Albrecht and M. Topič, *ACS Energy Lett.*, 2022, **7**, 1298–1307.

34 X. Guo, Q. Fan, J. Wu, G. Li, Z. Peng, W. Su, J. Lin, L. Hou, Y. Qin, H. Ade, L. Ye, M. Zhang and Y. Li, *Angew. Chem., Int. Ed.*, 2021, **60**, 2322–2329.

35 P. Chao, H. Chen, Y. Zhu, H. Lai, D. Mo, N. Zheng, X. Chang, H. Meng and F. He, *Adv. Mater.*, 2020, **32**, e1907059.

36 H. Sun, T. Liu, J. Yu, T.-K. Lau, G. Zhang, Y. Zhang, M. Su, Y. Tang, R. Ma, B. Liu, J. Liang, K. Feng, X. Lu, X. Guo, F. Gao and H. Yan, *Energy Environ. Sci.*, 2019, **12**, 3328–3337.

37 B. Fan, M. Li, D. Zhang, W. Zhong, L. Ying, Z. Zeng, K. An, Z. Huang, L. Shi, G. C. Bazan, F. Huang and Y. Cao, *ACS Energy Lett.*, 2020, **5**, 2087–2094.

38 R. Ma, T. Liu, Z. Luo, Q. Guo, Y. Xiao, Y. Chen, X. Li, S. Luo, X. Lu, M. Zhang, Y. Li and H. Yan, *Sci. China: Chem.*, 2020, **63**, 325–330.

39 Z. Zhang, Y. Li, G. Cai, Y. Zhang, X. Lu and Y. Lin, *J. Am. Chem. Soc.*, 2020, **142**, 18741–18745.

40 Z. Chen, W. Song, K. Yu, J. Ge, J. Zhang, L. Xie, R. Peng and Z. Ge, *Joule*, 2021, **5**, 2395–2407.

41 S. Lu, X. Guan, X. Li, W. E. I. Sha, F. Xie, H. Liu, J. Wang, F. Huang and W. C. H. Choy, *Adv. Energy Mater.*, 2015, **5**, 1500631.

42 S. Lu, H. Lin, S. Zhang, J. Hou and W. C. H. Choy, *Adv. Energy Mater.*, 2017, **7**, 1701164.

43 J. Kwon, M. J. Im, C. U. Kim, S. H. Won, S. B. Kang, S. H. Kang, I. T. Choi, H. K. Kim, I. H. Kim, J. H. Park and K. J. Choi, *Energy Environ. Sci.*, 2016, **9**, 3657–3665.

44 M. Zhang and Z. Lin, *Energy Environ. Sci.*, 2022, **15**, 3152–3170.

45 M. Kröger, S. Hamwi, J. Meyer, T. Riedl, W. Kowalsky and A. Kahn, *Appl. Phys. Lett.*, 2009, **95**, 123301.

46 J. Meyer, S. Hamwi, M. Kroger, W. Kowalsky, T. Riedl and A. Kahn, *Adv. Mater.*, 2012, **24**, 5408–5427.

47 S. Wu, M. Liu and A. K. Y. Jen, *Joule*, 2023, **7**, 484–502.

48 X. Zhou, H. Lai, T. Huang, C. Chen, Z. Xu, Y. Yang, S. Wu, X. Xiao, L. Chen, C. J. Brabec, Y. Mai and F. Guo, *ACS Energy Lett.*, 2022, **8**, 502–512.

49 X. Gu, X. Lai, Y. Zhang, T. Wang, W. L. Tan, C. R. McNeill, Q. Liu, P. Sonar, F. He, W. Li, C. Shan and A. K. K. Kyaw, *Adv. Sci.*, 2022, **9**, e2200445.

50 Y. Zhou, I. Poli, D. Meggiolaro, F. De Angelis and A. Petrozza, *Nat. Rev. Mater.*, 2021, **6**, 986–1002.

51 S. Qin, C. Lu, Z. Jia, Y. Wang, S. Li, W. Lai, P. Shi, R. Wang, C. Zhu, J. Du, J. Zhang, L. Meng and Y. Li, *Adv. Mater.*, 2022, **34**, e2108829.

52 G. E. Eperon, M. T. Hörantner and H. J. Snaith, *Nat. Rev. Chem.*, 2017, **1**, 0095.

53 R. A. Kerner, Z. Xu, B. W. Larson and B. P. Rand, *Joule*, 2021, **5**, 2273–2295.

54 T. Elmelund, B. Seger, M. Kuno and P. V. Kamat, *ACS Energy Lett.*, 2019, **5**, 56–63.

55 S. Mahesh, J. M. Ball, R. D. Oliver, D. P. McMeekin, P. K. Nayak, M. B. Johnston and H. J. Snaith, *Energy Environ. Sci.*, 2020, **13**, 258–267.

56 F. Peña-Camargo, P. Caprioglio, F. Zu, E. Gutierrez-Partida, C. M. Wolff, K. Brinkmann, S. Albrecht, T. Riedl, N. Koch, D. Neher and M. Stolterfoht, *ACS Energy Lett.*, 2020, **5**, 2728–2736.

57 M. Stolterfoht, C. M. Wolff, J. A. Márquez, S. Zhang, C. J. Hages, D. Rothhardt, S. Albrecht, P. L. Burn, P. Meredith, T. Unold and D. Neher, *Nat. Energy*, 2018, **3**, 847–854.

58 Y. M. Xie, Q. Yao, Z. Zeng, Q. Xue, T. Niu, R. Xia, Y. Cheng, F. Lin, S. W. Tsang, A. K. Y. Jen, H. L. Yip and Y. Cao, *Adv. Funct. Mater.*, 2022, **32**, 2112126.

59 H. X. Dang, K. Wang, M. Ghasemi, M.-C. Tang, M. De Bastiani, E. Aydin, E. Dauzon, D. Barrit, J. Peng, D.-M. Smilgies, S. De Wolf and A. Amassian, *Joule*, 2019, **3**, 1746–1764.

60 Y. M. Xie, Z. Zeng, X. Xu, C. Ma, Y. Ma, M. Li, C. S. Lee and S. W. Tsang, *Small*, 2020, **16**, e1907226.

61 C. U. Kim, J. C. Yu, E. D. Jung, I. Y. Choi, W. Park, H. Lee, I. Kim, D.-K. Lee, K. K. Hong, M. H. Song and K. J. Choi, *Nano Energy*, 2019, **60**, 213–221.

62 Q. A. Akkerman, G. Raino, M. V. Kovalenko and L. Manna, *Nat. Mater.*, 2018, **17**, 394–405.

63 W.-J. Yin, T. Shi and Y. Yan, *Appl. Phys. Lett.*, 2014, **104**, 063903.

64 W. J. Yin, T. Shi and Y. Yan, *Adv. Mater.*, 2014, **26**, 4653–4658.

65 X. Zheng, X. Wang, W. Li, Z. Liu, W. Ming, H. Wang, H. Wang, D. Li, B. Liu and C. Yang, *J. Phys. Chem. C*, 2021, **125**, 19551–19559.

66 T. Duong, Y. Wu, H. Shen, J. Peng, X. Fu, D. Jacobs, E. C. Wang, T. C. Kho, K. C. Fong, M. Stocks, E. Franklin, A. Blakers, N. Zin, K. McIntosh, W. Li, Y. B. Cheng, T. P. White, K. Weber and K. Catchpole, *Adv. Energy Mater.*, 2017, **7**, 1700228.

67 K. A. Bush, K. Frohna, R. Prasanna, R. E. Beal, T. Leijtens, S. A. Swifter and M. D. McGehee, *ACS Energy Lett.*, 2018, **3**, 428–435.

68 Z. Yang, A. Rajagopal, S. B. Jo, C. C. Chueh, S. Williams, C. C. Huang, J. K. Katahara, H. W. Hillhouse and A. K. Jen, *Nano Lett.*, 2016, **16**, 7739–7747.

69 M. Abdi-Jalebi, Z. Andaji-Garmaroudi, S. Cacovich, C. Stavrakas, B. Philippe, J. M. Richter, M. Alsari, E. P. Booker, E. M. Hutter, A. J. Pearson, S. Lilliu, T. J. Savenije, H. Rensmo, G. Divitini, C. Ducati, R. H. Friend and S. D. Stranks, *Nature*, 2018, **555**, 497–501.

70 J. Y. Ye, J. Tong, J. Hu, C. Xiao, H. Lu, S. P. Dunfield, D. H. Kim, X. Chen, B. W. Larson, J. Hao, K. Wang, Q. Zhao, Z. Chen, H. Hu, W. You, J. J. Berry, F. Zhang and K. Zhu, *Sol. RRL*, 2020, **4**, 2000082.

71 D. H. Kim, C. P. Muzzillo, J. Tong, A. F. Palmstrom, B. W. Larson, C. Choi, S. P. Harvey, S. Glynn, J. B. Whitaker, F. Zhang, Z. Li, H. Lu, M. F. A. M. van Hest, J. J. Berry, L. M. Mansfield, Y. Huang, Y. Yan and K. Zhu, *Joule*, 2019, **3**, 1734–1745.

72 Y. Zhou, Y. H. Jia, H. H. Fang, M. A. Loi, F. Y. Xie, L. Gong, M. C. Qin, X. H. Lu, C. P. Wong and N. Zhao, *Adv. Funct. Mater.*, 2018, **28**, 1803130.

73 R. E. Brandt, J. R. Poindexter, P. Gorai, R. C. Kurchin, R. L. Z. Hoye, L. Nienhaus, M. W. B. Wilson, J. A. Polizzotti, R. Sereika, R. Žaltauskas, L. C. Lee, J. L. MacManus-Driscoll, M. Bawendi, V. Stevanović and T. Buonassisi, *Chem. Mater.*, 2017, **29**, 4667–4674.

74 M. V. Kovalenko, L. Protesescu and M. I. Bodnarchuk, *Science*, 2017, **358**, 745–750.

75 S. Gharibzadeh, I. M. Hossain, P. Fassl, B. A. Nejand, T. Abzieher, M. Schultes, E. Ahlswede, P. Jackson, M. Powalla, S. Schäfer, M. Rienäcker, T. Wietler, R. Peibst, U. Lemmer, B. S. Richards and U. W. Paetzold, *Adv. Funct. Mater.*, 2020, **30**, 1909919.

76 D. Wang, H. Guo, X. Wu, X. Deng, F. Li, Z. Li, F. Lin, Z. Zhu, Y. Zhang, B. Xu and A. K. Y. Jen, *Adv. Funct. Mater.*, 2021, **32**, 2107359.

77 Y. Zhou, F. Wang, Y. Cao, J. P. Wang, H. H. Fang, M. A. Loi, N. Zhao and C. P. Wong, *Adv. Energy Mater.*, 2017, **7**, 1701048.

78 T. Bu, J. Li, Q. Lin, D. P. McMeekin, J. Sun, M. Wang, W. Chen, X. Wen, W. Mao, C. R. McNeill, W. Huang, X.-L. Zhang, J. Zhong, Y.-B. Cheng, U. Bach and F. Huang, *Nano Energy*, 2020, **75**, 104917.

79 C. Chen, Z. Song, C. Xiao, D. Zhao, N. Shrestha, C. Li, G. Yang, F. Yao, X. Zheng, R. J. Ellingson, C.-S. Jiang, M. Al-Jassim, K. Zhu, G. Fang and Y. Yan, *Nano Energy*, 2019, **61**, 141–147.